

Hamiltonian approach to QCD in Coulomb gauge: Gribov's confinement scenario at work*

H. Reinhardt^{1,a}, G. Burgio¹, D. Campagnari¹, M. Quandt¹, P. Vastag¹, H. Vogt¹, and E. Ebadati¹

¹ *Universität Tübingen
 Institut für Theoretische Physik
 Auf der Morgenstelle 14
 D-72076 Tübingen
 Germany*

Abstract. I will review essential features of the Hamiltonian approach to QCD in Coulomb gauge showing that Gribov's confinement scenario is realized in this gauge. For this purpose I will discuss in detail the emergence of the horizon condition and the Coulomb string tension. I will show that both are induced by center vortex gauge field configurations, which establish the connection between Gribov's confinement scenario and the center vortex picture of confinement. I will then extend the Hamiltonian approach to QCD in Coulomb gauge to finite temperatures, first by the usual grand canonical ensemble and second by the compactification of a spatial dimension. I will present results for the pressure, energy density and interaction measure as well as for the Polyakov loop.

1 Introduction

V. N. Gribov's investigation of the problem of gauge fixing in Yang–Mills theory has led to a novel picture of confinement. In this scenario confinement comes about due to the field configurations near the Gribov horizon, which give rise to an infrared diverging ghost form factor. This approach was worked out in more detail and developed further by D. Zwanziger and is now referred to as the Gribov–Zwanziger confinement mechanism [1, 2]. In my talk, I will show that this picture is realized in the Hamiltonian approach to Yang–Mills theory in Coulomb gauge. Gribov already pointed out that in Coulomb gauge the use of the Hamiltonian approach may be advantageous over the usual functional integral approach and this, indeed, turns out to be the case. The variational approach to the Hamilton formulation of QCD in Coulomb gauge developed in refs. [3, 4] has proven to be much more efficient than the formulation of QCD in Coulomb gauge by means of the functional integral approach [5]. In my talk I will concentrate on a few aspects of the Hamiltonian approach to QCD in Coulomb gauge. I will discuss in detail the emergence of the horizon condition which is the core of the Gribov–Zwanziger confinement scenario. Furthermore, I will show that the Coulomb string tension is not related to the temporal but to the spatial Wilsonian string tension. I will extend then

*Talk given by H. Reinhardt at "5th International Conference on New Frontiers in Physics", 6-14 July 2016, Kolymbari, Greece.

^ae-mail: hugo.reinhardt@uni-tuebingen.de

the Hamiltonian approach to finite temperatures, first by means of the grand canonical ensemble and second by compactification of a spatial dimension.

2 Hamiltonian approach to Yang–Mills theory in Coulomb gauge at $T = 0$

After canonical quantization and implementation of Gauß’s law in Weyl and Coulomb gauge, the gauge fixed Yang–Mills Hamiltonian reads [6]

$$H = \frac{1}{2} \int d^3x \left(J^{-1}[A] \Pi^a(\mathbf{x}) \cdot J[A] \Pi^a(\mathbf{x}) + \mathbf{B}^a(\mathbf{x}) \cdot \mathbf{B}^a(\mathbf{x}) \right) + H_C. \quad (1)$$

Here

$$\mathbf{B}_k^a(\mathbf{x}) = \varepsilon_{klm} \left(\partial_l A_m^a(\mathbf{x}) - \frac{g}{2} f^{abc} A_l^b(\mathbf{x}) A_m^c(\mathbf{x}) \right) \quad (2)$$

is the non-Abelian magnetic field, $\Pi_k^a(\mathbf{x}) = \delta / (i \delta A_k^a(\mathbf{x}))$ is the momentum operator, which represents the color electric field and

$$J[A] = \text{Det}(-\hat{\mathbf{D}} \cdot \partial), \quad \hat{\mathbf{D}}_k^{ab}(\mathbf{x}) = \delta^{ab} \partial_k^x + g \hat{A}_k^{ab}(\mathbf{x}) \quad (3)$$

is the Faddeev–Popov determinant, where $\hat{A}_k^{ab} = f^{acb} A_k^c$ is the gauge field in the adjoint representation. Furthermore,

$$H_C = \frac{1}{2} \int d^3x \int d^3y J[A]^{-1} \rho^a(\mathbf{x}) J[A] \left[(-\hat{\mathbf{D}} \cdot \partial)^{-1} (-\partial^2) (-\hat{\mathbf{D}} \cdot \partial)^{-1} \right]^{ab}(\mathbf{x}, \mathbf{y}) \rho^b(\mathbf{y}) \quad (4)$$

is the so-called Coulomb term, which arises from the kinetic energy of the longitudinal part of the momentum operator after resolving Gauß’s law. Here,

$$\rho^a(\mathbf{x}) = -f^{abc} \mathbf{A}^b(\mathbf{x}) \cdot \boldsymbol{\Pi}^c(\mathbf{x}) + \rho_m^a(\mathbf{x}) \quad (5)$$

is the color charge density, where the first term on the right-hand side is the contribution of the gauge field itself while the last term, ρ_m , refers to the matter fields. Due to the implementation of Coulomb gauge the scalar product between wave functionals

$$\langle \phi | \dots | \psi \rangle = \int \mathcal{D}A J[A] \phi^*[A] \dots \psi[A] \quad (6)$$

is defined by the functional integral over transversal gauge fields with the Faddeev–Popov determinant (3) in the integration measure representing the Jacobian of the change of variables from “Cartesian” to “curvilinear” variables in Coulomb gauge. With the gauge fixed Hamiltonian (1) one has to solve the stationary Schrödinger equation $H\psi[A] = E\psi[A]$ for the vacuum wave functional $\psi[A]$. Once $\psi[A]$ is known, all observables and correlation functions can, in principle, be calculated. This has been attempted by means of the variational principle using Gaussian type ansätze for the vacuum wave functional [7, 8]. However, the first attempts did not properly include the Faddeev–Popov determinant, which turns out to be crucial in order to describe the confinement properties of the theory. Below, I am discussing the variational approach developed in refs. [3, 4], which differs from previous attempts by the ansatz for the vacuum wave functional, the treatment of the Faddeev–Popov determinant and, equally important, in the renormalization, see ref. [9] for further details.

Figure 1: Dyson–Schwinger equation for the ghost propagator.

2.1 Variational solution of the Schrödinger equation

The ansatz for the vacuum wave functional is inspired by the quantum mechanics of a particle in a spherically symmetric potential for which the ground state wave functional reads $\psi(r) = u(r)/r$ where the radial wave functional $u(r)$ satisfies a usual one-dimensional Schrödinger equation and r represents (the square root of the radial part of) the Jacobian of the transformation from the Cartesian to spherical coordinates. Our ansatz for the vacuum wave functional is given by

$$\psi[A] = \frac{1}{\sqrt{J[A]}} \exp \left[-\frac{1}{2} \int d^3x \int d^3y A_k^a(\mathbf{x}) \omega(\mathbf{x}, \mathbf{y}) A_k^a(\mathbf{y}) \right]. \quad (7)$$

The inclusion of the pre-exponential factor has the advantage that it eliminates the Faddeev–Popov determinant from the integration measure in the scalar product (6). Furthermore, for the wave function (7) the gluon propagator is given up to a factor of $\frac{1}{2}$ by the inverse of the variational kernel $\omega(\mathbf{x}, \mathbf{y})$. It turns out that in the Yang–Mills sector the Coulomb term H_C (4) can be ignored. Calculating the expectation value of the remaining parts of the Yang–Mills Hamiltonian (1) with the wave functional (7) up to two loops, the minimization of the energy density with respect to $\omega(\mathbf{x}, \mathbf{y})$ yields the following gap equation in momentum space¹

$$\omega^2(k) = \mathbf{k}^2 + \chi^2(k) + c, \quad (8)$$

where c is a finite renormalization constant resulting from the tadpole and

$$\chi_{kl}^{ab}(\mathbf{x}, \mathbf{y}) = -\frac{1}{2} \left\langle \psi \left| \frac{\delta^2 \ln J[A]}{\delta A_k^a(\mathbf{x}) \delta A_l^b(\mathbf{y})} \right| \psi \right\rangle \quad (9)$$

represents the ghost loop. This can be expressed in terms of the ghost propagator

$$G(\mathbf{x}, \mathbf{y}) = \langle \psi | (-\hat{\mathbf{D}} \cdot \partial)^{-1}(\mathbf{x}, \mathbf{y}) | \psi \rangle, \quad (10)$$

which is evaluated with the vacuum wave functional (7) in an approximate way resulting in a Dyson–Schwinger equation for the form factor

$$d(\mathbf{k}) = g \mathbf{k}^2 G(\mathbf{k}) \quad (11)$$

of the ghost propagator which is diagrammatically illustrated in fig. 1. This equation has to be solved together with the gap equation (8). The numerical solutions are shown in fig. 2.

¹Due to translational and rotational invariance, kernels such as $\omega(\mathbf{x}, \mathbf{y})$ can be Fourier transformed as

$$\omega(\mathbf{x}, \mathbf{y}) = \int \frac{d^3k}{(2\pi)^3} e^{i\mathbf{k} \cdot (\mathbf{x} - \mathbf{y})} \omega(k),$$

where the new kernel in momentum space depends on $k = |\mathbf{k}|$ only. For simplicity, we will use the same symbol for the kernel in position and momentum space and go back and forth between both representations with impunity.

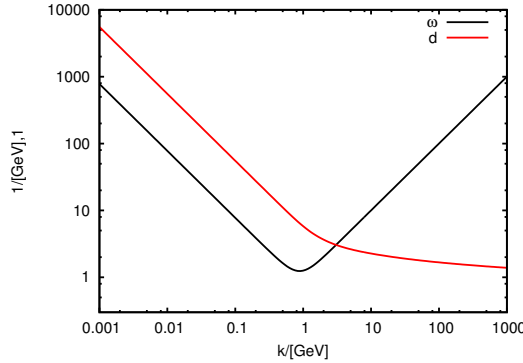


Figure 2: Numerical solution of the coupled gap equation for ω (8) and Dyson–Schwinger equation for the ghost form factor d for the renormalization constant $c = 0$ [10].

2.2 Physical implications of the ghost form factor

The ghost form factor expresses the deviation of Yang–Mills theory from QED. Dyson–Schwinger equations are functional differential equations and their solutions are uniquely determined after providing appropriate boundary conditions. In the present case the so-called horizon condition

$$d^{-1}(0) = 0 \quad (12)$$

is assumed, which is the key point in Gribov’s confinement scenario.

Alternatively to the variational approach, one can indirectly determine the vacuum wave functional by solving the functional renormalization group flow equations for the various propagators and functions of the Hamiltonian approach. Restricting the flow equations to those for the ghost and gluon propagators, one finds for the ghost form factor the result shown in fig. 3. Starting with a constant ghost form factor in the ultraviolet, the ghost form factor develops an infrared singularity as the momentum cutoff of the flow equation tends to zero. This is nicely seen in fig. 3 (b), which shows a cut through fig. 3 (a) at fixed renormalization group scale k .

Let us also mention that the horizon condition (12) need not be assumed in the case of $D = 2 + 1$ dimensions, where it is a necessary consequence of the coupled equations for the ghost and gluon propagators obtained with the variational principle. Finally, the horizon condition (12) is also seen in the lattice data for the ghost form factor shown in fig. 4.

Coulomb gauge is called a physical gauge since in QED the remaining transversal components are the gauge invariant degrees of freedom. This is not the case for Yang–Mills theory. However, Coulomb gauge can be viewed as a physical gauge also in the case of Yang–Mills theory in the sense that the inverse ghost form factor in Coulomb gauge represents the dielectric function of the Yang–Mills vacuum [13]

$$\epsilon(k) = d^{-1}(k). \quad (13)$$

The horizon condition (12) guarantees that this function vanishes in the infrared, $\epsilon(k = 0) = 0$. This implies that the Yang–Mills vacuum is a perfect color dielectricum, i.e. a dual superconductor. In this way the Hamiltonian approach in Coulomb gauge relates Gribov’s confinement scenario to the dual Meißner effect, a confinement mechanism realized through the condensation of magnetic monopoles and proposed by Mandelstam and ’t Hooft [14, 15]. The dielectric function obtained here as inverse

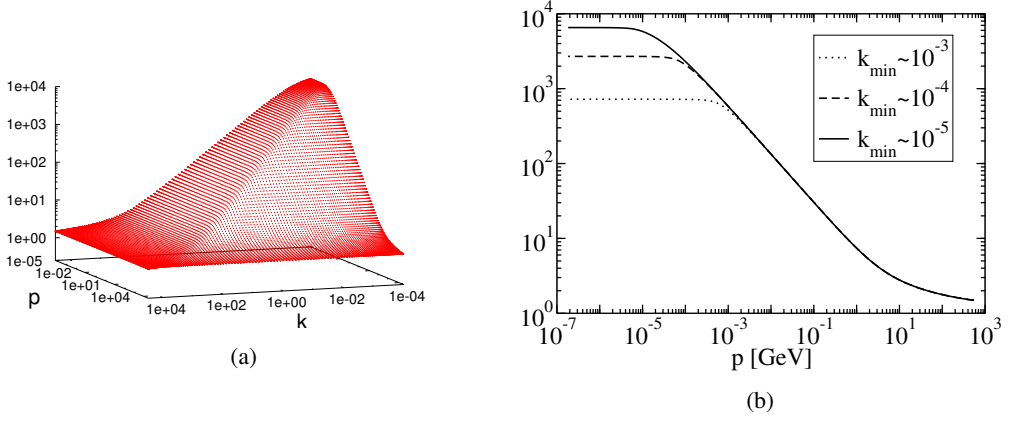


Figure 3: (a) The ghost form factor obtained in ref. [11] from the solution of the renormalization group flow equations. Here p represents the momentum variable of the ghost form factor while k is the infrared momentum cutoff of the flow equations. (b) Cuts through subfigure (a) at various values of the momentum scale k of the flow equations.

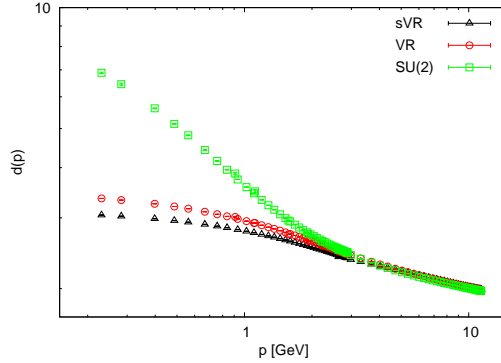


Figure 4: The ghost form factor in Coulomb gauge calculated on the lattice in ref. [12] (green symbols). The red and black symbols show the results obtained for the ghost form factor when all center vortices or the spatial center vortices are removed from the ensemble of gauge field configurations, see text.

ghost form factor is also in accord with the phenomenological bag model picture of hadrons. Inside the hadron, i.e. at small distance, the dielectric function is that of a normal vacuum while outside the physical hadrons the vanishing of the dielectric constant implies the absence of free charges by Gauß's law.

One may now ask, what field configurations induce the horizon condition and thus confinement? Given the relation of Gribov's confinement scenario to the dual superconductor, we expect magnetic monopoles to play a substantial role. Lattice calculations carried out in the so-called indirect maximum center gauge, which contains the maximum Abelian gauge in an intermediate step, show that magnetic monopoles are tied to center vortices. The latter are string-like gauge field configurations

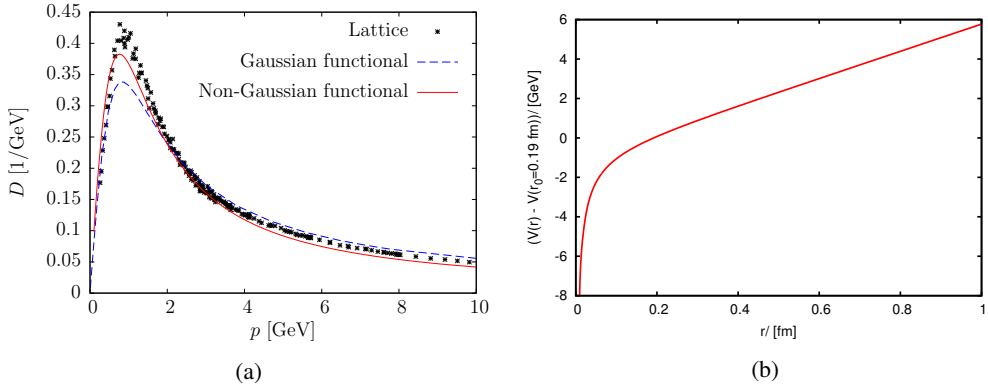


Figure 5: (a) The static gluon propagator in Coulomb gauge calculated on the lattice for SU(2) gauge theory (crosses). The dashed and the full curves show the result of the variational calculation using, respectively, a Gaussian and non-Gaussian ansatz for the vacuum wave functional. (b) The non-Abelian Coulomb potential (16) obtained in the variational approach [10].

for which the Wilson loop equals a non-trivial center element of the gauge group, provided the loop has non-trivially linking with the center vortex string. When the center vortex content of the gauge field configurations is removed, which can be done on the lattice, one finds that the Wilsonian string tension and thus confinement disappears [16]. Figure 4 shows the ghost loop obtained on the lattice when the center vortices are removed from the ensemble of gauge field configurations [12]. The ghost loop becomes infrared flat and the horizon condition is lost. This shows that center vortices induce the horizon condition which is the corner stone of Gribov's confinement scenario. This also shows that Gribov's confinement scenario is tied to the center vortex picture of confinement. This is in accord with the observation that center vortices and magnetic monopoles are located on the Gribov horizon of Coulomb gauge [17].

2.3 Comparison with lattice calculation

Let us now compare the results of the variational solution with lattice calculations [18]. Figure 5 (a) shows the gluon propagator of Coulomb gauge obtained in SU(2) gauge theory. It is remarkable that the lattice data can be nicely fitted by Gribov's formula [1]

$$\omega(p) = \sqrt{p^2 + \frac{M^4}{p^2}} \quad (14)$$

where M is the so-called Gribov mass. The variational calculations reproduce the infrared behavior of the lattice propagator perfectly and are also in reasonably agreement with the lattice data in the ultraviolet. However, in the mid-momentum regime some strength is missing in the variational calculation. This missing strength is the result of the Gaussian type ansatz for the vacuum wave functional. In ref. [19], the ansatz for the vacuum wave functional was extended to include also cubic and quartic

terms of the gauge field in the exponent of the vacuum wave functional

$$\psi[A] \sim \exp[-S[A]], \quad (15a)$$

$$S[A] = \frac{1}{2} \int A \omega A + \frac{1}{3!} \int \gamma^{(3)} AAA + \frac{1}{4!} \int \gamma^{(4)} AAAA \quad (15b)$$

and one finds the full curve in fig. 5 (a), which gives a much better agreement with the lattice data in the mid-momentum regime.

2.4 The Coulomb string tension

So far we have ignored the Coulomb Hamiltonian H_C (4) which is reasonable in the Yang–Mills sector. However, this term becomes extremely important in the quark sector. Let us consider the piece of H_C quadratic in the color density of the matter fields ρ_m . From this term the Faddeev–Popov determinant drops out and its Yang–Mills vacuum expectation value provides the static potential for the matter fields

$$V_C(|\mathbf{x} - \mathbf{y}|) = g^2 \langle \psi | [(-\hat{\mathbf{D}} \cdot \partial)^{-1} (-\partial^2) (-\hat{\mathbf{D}} \cdot \partial)^{-1}] (\mathbf{x}, \mathbf{y}) | \psi \rangle, \quad (16)$$

which is referred to as the non-Abelian Coulomb potential. The Coulomb potential resulting from the variational approach is shown in fig. 5 (b). At small distance it behaves like an ordinary Coulomb potential but rises linearly at large distance with a coefficient given by the so-called Coulomb string tension σ_C , which can be shown to represent an upper bound to the Wilsonian string tension σ_W [20]. On the lattice one finds a value of $\sigma_C = 2 \dots 4 \sigma_W$ [12, 17, 21]. At finite temperatures the Wilsonian string tension σ_W splits into a spatial and a temporal one. Above the deconfinement phase transition, the temporal string tension σ_t vanishes while the spatial string tension σ_s even slightly increases with the temperature. On the lattice one finds that the temporal and spatial string tension are induced by the spatial and temporal, respectively, center vortex content of the gauge field. When one removes the spatial center vortices from the ensemble of gauge fields, the temporal string tension is untouched while the spatial string tension disappears. Figure 6 (a) shows the non-Abelian Coulomb potential calculated on the lattice. When one removes the spatial center vortices this Coulomb potential becomes infrared flat, i.e. the Coulomb string tension σ_C disappears. This shows that the Coulomb string tension is tied to the spatial (Wilsonian) string tension and not to the temporal one, because both are sensitive to the same underlying degrees of freedom (the spatial center vortices). Since the spatial string tension increases with the temperature above the critical temperature we should expect the same behavior for the Coulomb string tension. This, indeed, is observed on the lattice as can be seen from fig. 6 (b), where the quantity $p^4 V_C(p)$ is shown for various temperatures. As can be seen from this figure, the Coulomb string tension

$$\sigma_C = \lim_{p \rightarrow 0} p^4 V_C(p) \quad (17)$$

remains more or less constant as the temperature is increased from 0 to 1.5 times the critical temperature, and then increases strongly when further increasing the temperature to 3 times the critical one. This is in accordance with the temperature behavior of the spatial string tension found in lattice calculations [22].

The variational approach to Yang–Mills theory developed in refs. [3, 4] has also been extended to full QCD, see refs. [23–25]. Due to lack of time I will not consider the quark sector within my talk.

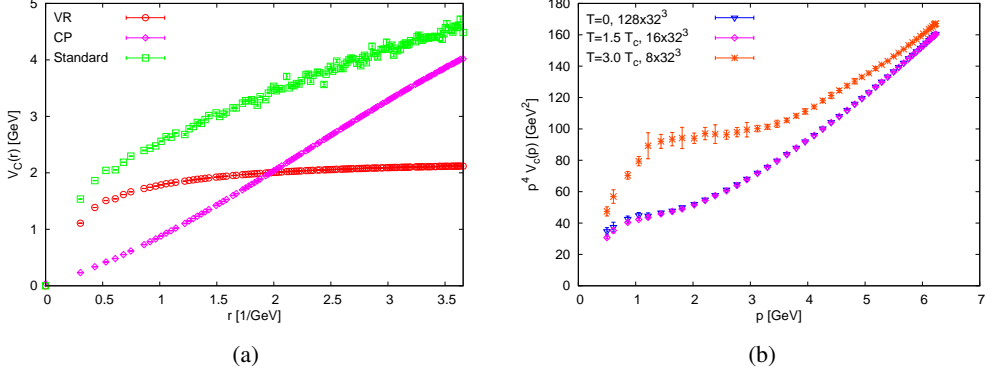


Figure 6: (a) Non-Abelian Coulomb potential V_C in coordinate space calculated on the lattice (green symbols). Red and violet symbols show the results obtained by vortex removal and center projection, respectively. (b) Measurements for the quantity $p^4 V_C(p)$ as function of the momentum p for various temperatures [12].

3 Hamiltonian approach to Yang–Mills theory at finite temperatures

3.1 Grand canonical ensemble

In refs. [26, 27], the variational approach to Yang–Mills theory in Coulomb gauge was extended to finite temperatures T by making a quasi-particle ansatz for the density matrix of the grand canonical ensemble with zero chemical potential

$$\tilde{D} = \exp(-\tilde{H}/T), \quad (18)$$

where \tilde{H} denotes the quasi-gluon (single-particle) Hamiltonian whose quasi-particle energies were determined by minimizing the free energy

$$F = \langle H \rangle_T - TS \rightarrow \min. \quad (19)$$

Here,

$$\langle \dots \rangle_T = \frac{\text{tr}(\tilde{D} \dots)}{\text{tr} \tilde{D}} \quad (20)$$

denotes the thermal expectation value of the grand canonical ensemble (i.e. the trace extends over the whole gluonic Fock space) and

$$S = -\text{tr} \left(\frac{\tilde{D}}{\text{tr} \tilde{D}} \ln \frac{\tilde{D}}{\text{tr} \tilde{D}} \right) = - \left\langle \ln \frac{\tilde{D}}{\text{tr} \tilde{D}} \right\rangle_T \quad (21)$$

is the usual entropy defined with the density matrix (18). The variational principle (19) has been solved in ref. [27] analogously to the one at zero temperature. Recently this approach has been used to calculate the pressure, energy density and interaction strength of SU(2) gluon dynamics [28]. The results are shown in fig. 7. The agreement with lattice data is not very impressive but one should keep in mind that these are microscopic self-consistent calculations.

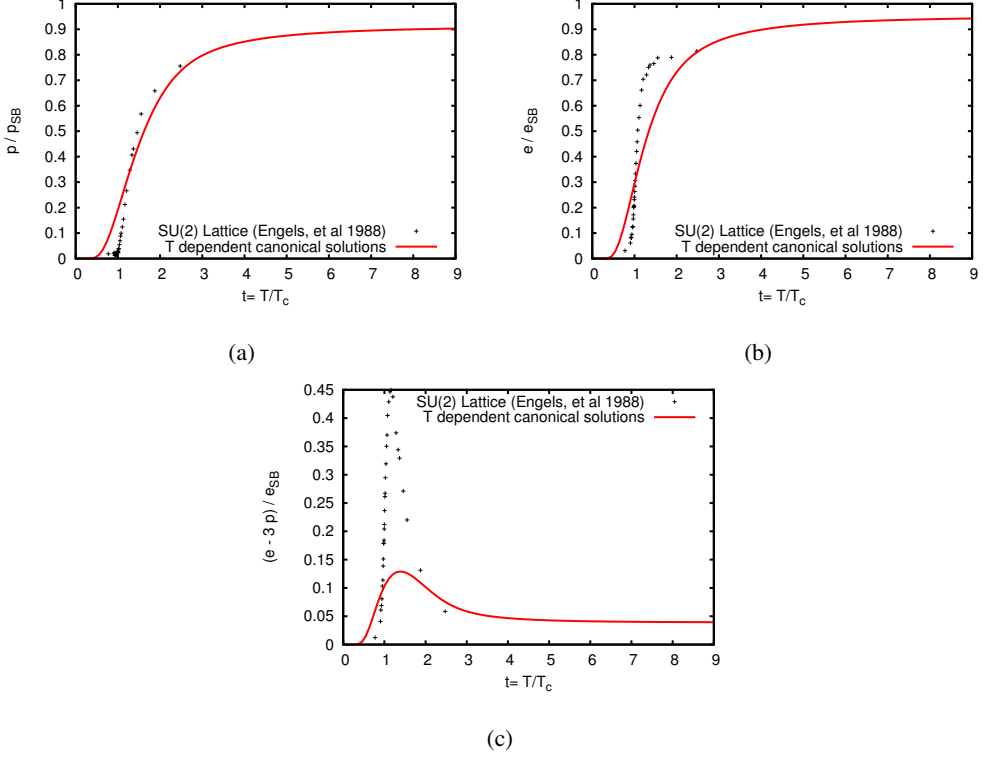


Figure 7: The (a) pressure, (b) energy density and (c) interaction strength of SU(2) gluon dynamics calculated in the finite temperature variational approach to Yang–Mills theory in Coulomb gauge developed in refs. [26, 27].

In ref. [29], gluon dynamics has been studied in a quasi-particle picture using Gribov’s formula (14) for the gluon quasi-particle energy. Thereby the Gribov mass was adjusted to reproduce the high temperature tail of the interaction strength yielding a Gribov mass of $M = 705$ MeV which is substantially smaller than the value $M = 880$ MeV found on the lattice [18]. It is therefore not surprising that the model calculation of ref. [29] did not properly describe the interaction strength in the low temperature region. If one wants to reproduce pressure, energy density or interaction strength of Yang–Mills theory within the quasi-particle model used in ref. [29], a temperature dependent Gribov mass is required. This is seen from the lattice calculation of the gluon propagator $D(p)$ at finite temperature presented in fig. 8, where the quantity $D(p)/p$ is shown. Assuming Gribov’s formula (14) for the gluon energy at all temperatures, this quantity reduces in the zero momentum limit to $1/(2M^2)$. As can be seen from fig. 8, the Gribov mass M does not change much as one increases the temperature from 0 to $1.5T_c$ but increases substantially when the temperature is further increased to 3 times the critical one.

3.2 Finite temperatures by compactification of a spatial dimension

There is a more efficient way to treat Yang–Mills theory at finite temperature within the Hamiltonian approach. The motivation comes from the Polyakov loop

$$P[A_0](x) = \frac{1}{d_r} \text{tr} P \exp \left[i \int_0^L dx^4 A_0(\mathbf{x}, x^4) \right], \quad (22)$$

where d_r denotes the dimension of the representation of the gauge group and L is the inverse temperature.² The expectation value of the Polyakov loop $\langle P[A_0] \rangle$ is an order parameter for confinement [31]. In the center symmetric confined phase this quantity vanishes while it approaches unity in the deconfined phase. This quantity cannot be calculated straightforwardly in the Hamiltonian approach due to the unrestricted time interval and the use of the Weyl gauge $A_0 = 0$. One can, however, exploit $O(4)$ invariance and interchange the Euclidean time axis with a spatial axis. The temporal (anti-)periodic boundary conditions to the fields become then spatial boundary conditions while the new (Euclidean) time axis has infinite extent, as is required for the Hamiltonian approach. As the result, the partition function is entirely given by the ground state calculated on the spatial manifold $\mathbb{R}^2 \times S^1(L)$ where L is again the inverse temperature. The whole thermodynamics is then encoded in the vacuum calculated on the partially compactified spatial manifold $\mathbb{R}^2 \times S^1(L)$. This approach has been worked out in ref. [32] and was used in refs. [33, 34] to calculate the Polyakov loop within the Hamiltonian approach.

In refs. [35, 36] it was shown that instead of using the expectation value of the Polyakov loop as order parameter of confinement one can also use the Polyakov loop of the expectation value $P[\langle A_0 \rangle]$ or the expectation value of the gauge field $\langle A_0(x) \rangle$ whereas the gauge field has to be in the Polyakov gauge, i.e. it has to be independent of the (Euclidean) time and diagonal in color space. Using this result it turns out that the most efficient way to obtain the Polyakov loop is to calculate the effective potential of a temporal background field a_0 fulfilling the Polyakov gauge and calculate the Polyakov loop from the minimum of this effective potential, say \bar{a}_0 . The quantity $P[\bar{a}_0]$ can then be used as alternative to $\langle P[A_0] \rangle$. This was done within the Hamiltonian approach in refs. [33, 34] using the finite temperature formulation of quantum field theory developed in ref. [32]. The color diagonal constant background field $\mathbf{a} = \mathbf{a}_3 t_3$ (t denotes the generator of the color group in the fundamental representation) has to be directed along the compactified spatial axis. Using the zero temperature gluon and ghost propagator as input one finds within this approach for $SU(2)$ the effective potential $e[a]$ shown in fig. 9 (a). The potential shows a second order phase transition. Using the Gribov mass of $M = 880$ MeV for fixing the scale one finds from the self-consistent (zero temperature) solution a critical temperature of $T_C = 269$ MeV.

Since the $SU(3)$ algebra consists of three $SU(2)$ algebras characterized by the three non-zero positive roots

$$\boldsymbol{\sigma} = (1, 0), \quad \left(\frac{1}{2}, \frac{1}{2} \sqrt{3} \right), \quad \left(\frac{1}{2}, -\frac{1}{2} \sqrt{3} \right) \quad (23)$$

the effective potential for $SU(3)$ is given by the following sum of $SU(2)$ potentials

$$e_{SU(3)}[a] = \sum_{\boldsymbol{\sigma} > 0} e_{SU(2)(\boldsymbol{\sigma})}[a], \quad (24)$$

²Recall that in the Euclidean functional integral approach, finite temperatures are introduced by compactifying the time axis.

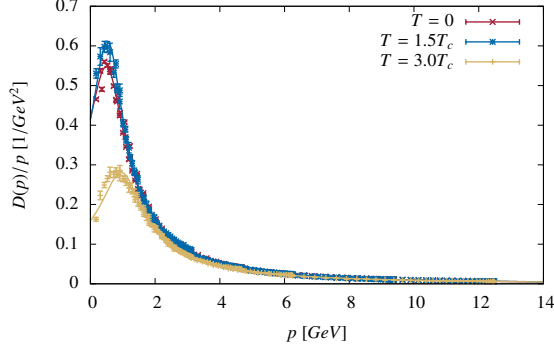


Figure 8: $D(p)/p$ for $T = 0, 1.5T_c$ and $3T_c$ [30].

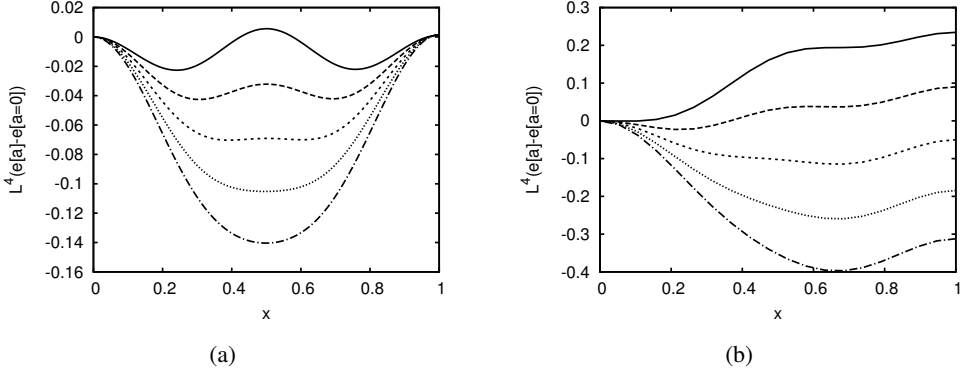


Figure 9: (a) The effective potential of the Polyakov loop (more precisely of the background field along the compactified spatial dimension) for the case of SU(2) for various temperatures (increasing from bottom to top) near the deconfinement phase transition; $x = \frac{a_3 L}{2\pi}$. (b) The $a_8 = 0$ section of the effective potential of the Polyakov loop for the gauge group SU(3) for various temperatures increasing from bottom to top, see also fig. 10.

where the sum runs over all positive non-zero roots given in eq. (23). SU(3) has two generators of the Cartan algebra (t_3, t_8). Therefore the effective potential of the Polyakov loop depends on two background fields a_3 and a_8 and is shown in fig. 10 for two temperatures, one below and one above the critical one. As one observes in these figures both for $T < T_c$ and $T > T_c$ an absolute minimum occurs for $a_8 = 0$. Cutting the effective potential along the $a_8 = 0$ axis one finds the temperature dependent potential shown in fig. 9 (b), which exhibits a first order phase transition. With a Gribov mass of $M = 880$ MeV as input one finds from the self-consistent (zero-temperature) solution a critical temperature of $T_c = 283$ MeV.

Finally, if one includes fermions the deconfinement phase transition is turned into a crossover for both SU(2) and SU(3) [37].

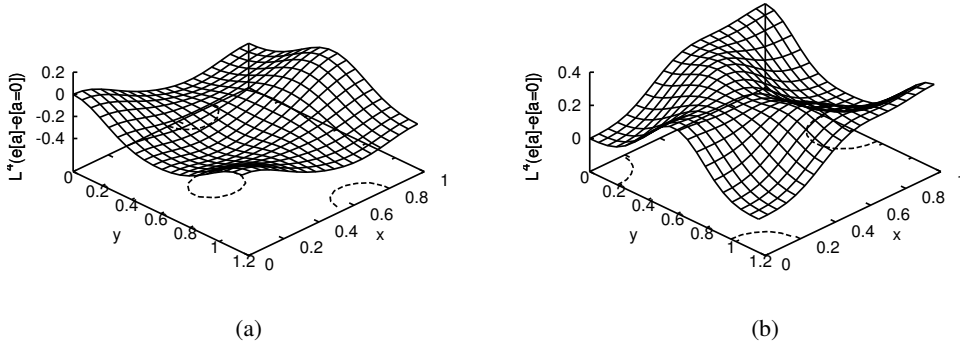


Figure 10: The effective potential of the Polyakov loop as function of the gauge fields along the Cartan generators a_3 and a_8 (a) for a temperature below the critical one and (b) for a temperature above the critical one; $x = \frac{a_3 L}{2\pi}$, $y = \frac{a_8 L}{2\pi}$.

4 Summary and Conclusions

In my talk I have summarized basic features of the Hamiltonian approach to Yang–Mills theory in Coulomb gauge. I have shown how the Gribov–Zwanziger confinement scenario is realized in this approach, and I have also established the connection with two alternative pictures of confinement, namely, the condensation of magnetic monopoles (dual Meißner effect) and the center vortex picture. In particular, I have shown that the Coulomb string tension is not related to the temporal but rather to the spatial Wilsonian string tension and hence has to increase with the temperature above the deconfinement phase transition. I have then extended the Hamiltonian approach to finite temperatures in two ways, first by means of the standard grand canonical ensemble and second by compactifying one spatial dimension. The latter formulation is advantageous since it does not require any assumption for the density operator of the grand canonical ensemble; instead the finite temperature theory is fully encoded in the vacuum state calculated on the partially compactified spatial manifold $\mathbb{R}^2 \times S^1(L)$. Within this approach the effective potential of the Polyakov loop was calculated and a second and first, respectively, order phase transition was found for the gauge group SU(2) and SU(3). These phase transitions turn into a crossover when the quarks are included. All these features are also corroborated by lattice calculations.

Acknowledgement

This work was supported by DFG under contract no. DFG-Re856/9-2.

References

- [1] V. N. Gribov, Nucl. Phys. **B139**, 1 (1978).
- [2] D. Zwanziger, Nucl. Phys. **B518**, 237 (1998).
- [3] C. Feuchter and H. Reinhardt, Phys. Rev. D **70**, 105021 (2004); arXiv:hep-th/0402106.
- [4] H. Reinhardt and C. Feuchter, Phys. Rev. D **71**, 105002 (2005); arXiv:hep-th/0408237.
- [5] P. Watson and H. Reinhardt, Phys. Rev. D **85**, 025014 (2012); arXiv:1111.6078.

- [6] N. H. Christ and T. D. Lee, Phys. Rev. D **22**, 939 (1980).
- [7] D. Schütte, Phys. Rev. D **31**, 810 (1985).
- [8] A. P. Szczepaniak and E. S. Swanson, Phys. Rev. D **65**, 025012 (2001); arXiv:hep-ph/0107078.
- [9] J. Greensite, H. Matevosyan, Š. Olejník, M. Quandt, H. Reinhardt and A. P. Szczepaniak, Phys. Rev. D **83**, 114509 (2011); arXiv:1102.3941.
- [10] D. Epple, H. Reinhardt and W. Schleifenbaum, Phys. Rev. D **75**, 045011 (2007); arXiv:hep-th/0612241.
- [11] M. Leder, J. M. Pawłowski, H. Reinhardt and A. Weber, Phys. Rev. D **83**, 025010 (2011); arXiv:1006.5710.
- [12] G. Burgio, M. Quandt, H. Reinhardt and H. Vogt, Phys. Rev. D **92**, 034518 (2015); arXiv:1503.09064.
- [13] H. Reinhardt, Phys. Rev. Lett. **101**, 061602 (2008); arXiv:0803.0504.
- [14] S. Mandelstam, Phys. Rep. **C23**, 245 (1976).
- [15] G. 't Hooft, Phys. Scr. **25**, 133 (1982).
- [16] P. de Forcrand and M. D'Elia, Phys. Rev. Lett. **82**, 4582 (1999); arXiv:hep-lat/9901020.
- [17] J. Greensite, Š. Olejník and D. Zwanziger, Phys. Rev. D **69**, 074506 (2004); arXiv:hep-lat/0401003.
- [18] G. Burgio, M. Quandt, H. Reinhardt, Phys. Rev. Lett. **102**, 032002 (2009); arXiv:0807.3291.
- [19] D. R. Campagnari and H. Reinhardt, Phys. Rev. D **82**, 105021 (2010); arXiv:1009.4599.
- [20] D. Zwanziger, Nucl. Phys. **B485**, 185 (1997); arXiv:hep-th/9603203.
- [21] A. Voigt, E.-M. Ilgenfritz, M. Müller-Preussker, A. Sternbeck, Phys. Rev. D **78**, 014501 (2008); arXiv:0803.2307.
- [22] G. Bali et al., Phys. Rev. Lett. **71**, 3059 (1993); arXiv:hep-lat/9306024.
- [23] M. Pak and H. Reinhardt, Phys. Lett. B **707**, 566 (2012); arXiv:1107.5263.
- [24] M. Pak and H. Reinhardt, Phys. Rev. D **88**, 125021 (2013); arXiv:1310.1797.
- [25] P. Vastag and H. Reinhardt, Phys. Rev. D **93**, 065003 (2016); arXiv:1512.06733.
- [26] H. Reinhardt, D. R. Campagnari and A. P. Szczepaniak, Phys. Rev. D **84**, 045006 (2011); arXiv:1107.3389.
- [27] J. Heffner, H. Reinhardt and D. R. Campagnari, Phys. Rev. D **85**, 125029 (2012); arXiv:1206.3936.
- [28] J. Heffner and H. Reinhardt, to be published
- [29] D. Zwanziger, Phys. Rev. Lett. **94**, 182301 (2005); arXiv:hep-ph/0407103.
- [30] H. Vogt, G. Burgio, M. Quandt and H. Reinhardt Proc. Sci. LATTICE2013, 363 (2014); arXiv:1311.5707.
- [31] B. Svetitsky, Phys. Rep. **132**, 1 (1986).
- [32] H. Reinhardt, arXiv:1604.06273.
- [33] H. Reinhardt and J. Heffner, Phys. Lett. B **718**, 2 (2012); arXiv:1210.1742.
- [34] H. Reinhardt and J. Heffner, Phys. Rev. D **88**, 045024 (2013); arXiv:1304.2980.
- [35] J. Braun, H. Gies and J. M. Pawłowski, Phys. Lett. B **684**, 262 (2010); arXiv:0708.2413.
- [36] F. Marhauser and J. M. Pawłowski, arXiv:0812.1144.
- [37] J. Heffner, H. Reinhardt and P. Vastag, to be published.